

## Flat-Bottom Strategy for Improved Accuracy in Protein Side-Chain Placements

Victor Wai Tak Kam and William A. Goddard III\*

*Materials and Process Simulation Center (MC-139-74), California Institute of Technology, Pasadena, California 91125*

Received May 28, 2008

**Abstract:** We present a new strategy for protein side-chain placement that uses flat-bottom potentials for rotamer scoring. The extent of the flat bottom depends on the coarseness of the rotamer library and is optimized for libraries ranging from diversities of 0.2 Å to 5.0 Å. The parameters reported here were optimized for forcefields using Lennard-Jones 12–6 van der Waals potential with DREIDING parameters but are expected to be similar for AMBER, CHARMM, and other forcefields. This *Side-Chain Rotamer Excitation Analysis Method* is implemented in the SCREAM software package. Similar scoring function strategies should be useful for ligand docking, virtual ligand screening, and protein folding applications.

### 1. Introduction

In developing general predictive approaches for structures of membrane proteins<sup>1–3</sup> (Membstruk), we found that current available side-chain placement methods, e.g. SCWRL, did not provide sufficiently accurate results to determine the helix-helix relative orientations within the membrane. Consequently, we developed the SCREAM approach reported here, which we have found to lead to dramatically improved protein structures. In this paper, we validate SCREAM against standard libraries of crystal structures. In a subsequent paper, we will report the accuracy of SCREAM in predicting stable membrane structures (where unfortunately there are very few accurate X-ray structures).

Side-chain placement methods play a major role in recent applications in the field of computational molecular biology: from protein design,<sup>4–6</sup> flexible ligand docking,<sup>7</sup> and loop-building<sup>8</sup> to prediction of protein structures.<sup>9</sup> Much attention has been paid to this important problem, which is difficult because it is in a category of problems known as NP-hard,<sup>10</sup> for which no efficient algorithm is known to exist. Since the groundbreaking work by Ponder and Richards,<sup>11</sup> many approaches have been developed, including mean-field approximation,<sup>12,13</sup> Monte Carlo algorithms,<sup>14,15</sup> and Dead-End Elimination (DEE).<sup>16–19</sup> In practice, however, studies have also concluded that the combinatorial issue may not be as severe as originally thought.<sup>20,21</sup> Compared to the

placement methods and rotamer libraries, scoring functions have not been studied as extensively.<sup>22–24</sup> The focus of this paper is on the scoring function.

The scoring function is based on the all-atom forcefield DREIDING<sup>25</sup> which includes an explicit hydrogen bond term. The use of a rotamer library is widely used in side-chain prediction methods, and many authors have introduced quality rotamer libraries<sup>21,26,27</sup> since the Ponder library. To account for the discreteness of rotamer libraries, several approaches have been introduced, such as reducing van der Waals radii,<sup>28,29</sup> capping of repulsion energy,<sup>30</sup> rotamer minimization,<sup>14,31</sup> and the use of subrotamer ensembles for each dominant rotamer.<sup>32</sup> We introduce a flat-bottom region for the van der Waals (VDW) 12–6 potential and the DREIDING hydrogen bond term (12–10 with a cosine angle term). The width of the flat bottom depends on the specific atom of each side chain as well as the coarseness of the underlying rotamer library used.

We show in this study that accuracy can be improved substantially by introducing the flat-bottom potential and in a systematic way. In addition to showing that placement accuracy is dependent upon the number of rotamers used in a library, we find that it is possible for suitably chosen energy functions to compensate the use of coarser rotamer libraries. We demonstrate a high overall accuracy in side-chain placement and make a comparison to the popular side-chain placement program SCWRL.<sup>33</sup>

\* Corresponding author e-mail: wag@wag.caltech.edu.

Table 1

diversity	starting	0.2 Å	0.6 Å	1.0 Å	1.4 Å	1.8 Å	2.2 Å	3.0 Å	5.0 Å	All-Torsion
rotamer count	35828	14755	3195	1014	378	214	136	84	44	382

## 2. Materials and Methods

**2.1. Preparation of Rotamer Libraries.** Rotamer libraries of various diversities are derived from the complete coordinate rotamer library of Xiang.<sup>21</sup> We added hydrogens to the rotamers and considered both  $\delta$  and  $\epsilon$  versions in the case for histidines. CHARMM charges are used throughout.<sup>34</sup> Since the Xiang library was based on crystal structure data, we minimized each of the conformations so that the internal energies will be consistent with subsequent energy evaluations of the proteins. To do this we placed each side chain on a template backbone (Ala-X-Ala in the extended conformation) and did 10 steps conjugate gradient minimization using the DREIDING forcefield.

We generated rotamer libraries of varying coarseness by a clustering procedure, using the heavy atom rmsd between minimized rotamers as the metric. Starting with the closest rotamers, we eliminated those within the specific threshold rmsd value choosing always the rotamer with the lowest minimized DREIDING energy. This threshold rmsd value is defined as the *diversity* of the resulting library. To ensure that rotamers can make proper hydrogen bonds, each side-chain conformation for serine, threonine, and tyrosine was repeated with each possible polar hydrogen position. Thus, for serine and threonine, the three  $sp^3$  position hydrogens were added to the hydroxyl oxygen, while for tyrosine, we add the out-of-plane OH bonds 90 degrees from the phenyl ring in addition to two  $sp^2$  positions in the plane. The final number of rotamers for libraries of different diversities is shown in Table 1.

In addition, we constructed the “*all-torsion*” rotamer library in which one rotamer for each major torsional angle (120 degrees for  $sp^3$  anchor atoms, 180 degrees for  $sp^2$  anchor atoms) was included. The angles were obtained from the backbone independent rotamer library from Dunbrack<sup>35</sup> and built using the same procedure as described above.

All our rotamer libraries are backbone independent.

**2.2. Preparation of Structures for Validation of SCREAM.** We considered three sets of protein for validating and training SCREAM.

- Xiang: Xiang<sup>21</sup> considered 33 proteins for testing their method for developing libraries of side-chain conformations: 1aac, 1aho, 1b9o, 1c5e, 1c9o, 1cbn, 1cc7, 1cex, 1cku, 1ctj, 1cz9, 1czp, 1d4t, 1eca, 1igd, 1lix, 1mf, 1plc, 1qj4, 1ql0, 1qlw, 1qnj, 1qq4, 1qtn, 1qtw, 1qu9, 1rcf, 1vfy, 2pth, 3lzt, 5p21, 5pti, and 7rsa. We have tested SCREAM for exactly these cases.

- Liang: Liang<sup>22,36</sup> considered 15 proteins for testing their method for scoring functions for choosing side-chain conformations. Of these, the 10 were not in the Xiang set are denoted as the Liang set: 1bpi, 1isu, 1ptx, 1xnb, 256b, 2erl, 2hbg, 2ihl, 5rxn, and 9rnt. The proteins that overlap with the Xiang set are not included.

- Other: In addition we included 10 proteins with resolution not worse than 1.8 Å from the SCWRL data set: 1a8d, 1bfd,

1bgf, 1c3d, 1ctf, 1ctj, 1moq, 1rzi, 1svy, and 1yge. Here we ignored structures with ligands or missing residues or which had a sequence identity of more than 50% with the Xiang or Liang sets. As will be described in later sections, this set is used only for deriving the  $\sigma$ -values and side-chain placement parameters.

For each of these 53 proteins, the raw atom coordinates were downloaded from the PDB database. Hydrogens were added using WHATIF<sup>37</sup> and ligands were typed using PRODRUG.<sup>38</sup> Manual typing of ligands were carried out in cases where they cannot be typed by PRODRUG (~10 cases). Waters, solvents, and metals were kept when present.

These structures were then minimized (100 conjugate gradient steps) using the DREIDING forcefield. In all cases, the minimized structures differed by less than 0.3 Å total rmsd compared to the original crystal structures. All metals, prolines, cysteines in disulfide bonds, and side chains in coordination with metals were kept fixed throughout side-chain placement calculations.

**2.3. Surface Area Calculations.** Which residues were considered as buried or exposed was determined from the Solvent Accessible Surface Area (SASA), using a probe of radius 1.4 Å. The reference for fully exposed surface area for each side-chain type is a fully extended tripeptide in the form of Ala-X-Ala. A side chain with >20% SASA compared with the reference SASA was considered exposed. This percentage is smaller than the typical 50% level in the literature—around 25% for the Xiang set and 39% for the Liang set because we include solvent molecules as part of the structure.

**2.4. Positioning of Side Chains.** Placement of the rotamers on the backbone is decided by the coordinates of the C, C $\alpha$ , N backbone atoms plus the C $\beta$  atom. To specify the position of the C $\beta$  atom we use the coordinates with respect to C, C $\alpha$ , N based on the statistics gathered from the HBPLUS protein set (see above). This involves three parameters:

1. The angle of the C $\alpha$ -C $\beta$  bond from the bisector of the C-C $\alpha$ -N angle: 1.81° (from the HBPLUS protein set)
2. The angle of the C $\alpha$ -C $\beta$  bond with the C-C $\alpha$ -N plane: 51.1° (from the HBPLUS protein set); and
3. The C $\alpha$ -C $\beta$  bond length: 1.55 Å (average value from the other protein set).

Thus the C $\beta$  atom will generally have a different position from the crystal C $\beta$  position. As in common practice in the literature, we did not include this C $\beta$  deviation in the rmsd calculations.

**2.5. Combinatorial Placement Algorithm.** The SCREAM combinatorial placement algorithm consists of three stages: self-energy calculation for rotamers, clash elimination, and further optimization of side chains.

**2.5.1. Stage 1: Rotamer Self-Energy Calculation.** The all atom forcefield DREIDING<sup>25</sup> was used to calculate the interactions between atoms, with a modification to be

described in the scoring function section. The internal energy contributions  $E_{\text{internal}}$  (bond, angle, and torsion terms and nonbonds that involve only the side-chain atoms) were precalculated and stored in the rotamer library. For each residue to be replaced, the interaction energy ( $E_{\text{sc-fixed}}$ ) was calculated for each rotamer interacting with just the protein backbone and fixed residues (all fixed atoms). The sum of these two terms is the empty lattice energy ( $E_{\text{EL}}$ ) of a rotamer in the absence of all other side chains to be replaced

$$E_{\text{EL}} = E_{\text{internal}} + E_{\text{sc-fixed}}$$

We use the term ground-state to refer to the rotamer with the lowest  $E_{\text{EL}}$  energy. All other rotamer states are termed excited states. Excited states with an energy 50 kcal/mol above the ground-state were discarded from the rotamer list for the remaining calculations.

**2.5.2. Stage 2: Clash Elimination.** Eisenmenger et al.<sup>20</sup> showed that the side-chain-backbone interaction accounts for the geometries of 74% of all core side chains and 53% of all side chains. Thus, the ground-state of each side chain was taken as the starting structure. Of course, this structure might have severe VDW clashes between side chains since no interaction between side chains has been included. Elimination of these clashes was done as follows. A list of clashes of all ground-state pairs, above a default threshold of 25 kcal/mol, was sorted by their clashing energies. The pair (A, B) with the worst clash was then subjected to rotamer optimization by considering all pairs of rotamers and selecting the lowest energy to form a super-rotamer with a new energy

$$E_{\text{tot}}(A, B) = E_{\text{self}}(A) + E_{\text{self}}(B) + E_{\text{Int.}}(A, B) \equiv E_{\text{self}}(AB)$$

where  $E_{\text{Int.}}$  indicates the interaction energy between rotamer A and rotamer B, which was the only energy calculation done at this step since the  $E_{\text{EL}}$  terms were calculated in Stage 1. The ground-state for this super rotamer now replaced the rotamer pair in the original structure. Since large side chains such as ARG and LYS may have as many as Y rotamers for the 1.0 Å library, we limited the number of pairs to be calculated explicitly to 1000, which we selected based upon the sum of the empty lattice energies. Of these interaction pairs we kept the ones with interaction energies below Z.

After resolving a clash, we considered the lowest X rotamer pairs from the above calculation as a super residue. Thus, subsequent clash resolution, say between residue C and residue A, will consider interactions of all side chains of C with the X (A,B) rotamer pairs. Now the spectrum of interaction energies treats (A,B) as a super rotamer so that the (C, (A,B)) energy spectrum is treated the same as for a simple rotamer pair with the spectrum:

$$\begin{aligned} E_{\text{tot}}(A, B, C) &= E_{\text{self}}(A) + E_{\text{self}}(B) + E_{\text{self}}(C) + E_{\text{Int.}}(A, B) + \\ &\quad E_{\text{Int.}}(A, C) + E_{\text{Int.}}(B, C) \\ &= E_{\text{self}}(AB) + E_{\text{self}}(C) + E_{\text{Int.}}(A, C) + E_{\text{Int.}}(B, C) \\ &\equiv E_{\text{self}}(AB) + E_{\text{self}}(C) + E_{\text{Int.}}(AB, C) \end{aligned}$$

This process continued by generating a new list of clashing residue pairs including the new (A,B,C), resolving the next worst clash as above. The procedure was repeated until no

further clashes were identified between two rotamers or superrotamers.

**2.5.3. Stage 3: Final Doublet Optimization.** It is possible for some clashes to remain after Stage 2, since the number of rotamers pair evaluations is capped (at 1000) and also the numbers of rotamers in a super-rotamer (20). To solve this problem, the structure from the end of stage 2 was further optimized. Side-chain pairs (termed *doublets*) were now ordered in decreasing energies in the presence of all other side chains, and one iteration round of local optimization on those residue pairs was performed in that order. Any residue that had already been examined in this stage as part of a doublet was eliminated from further doublet examination. Always, the doublet with the lowest overall energy was kept.

**2.5.4. Stage 4: Final Singlet Optimizations.** The structure would undergo one final round of optimization, where all residues were examined one at a time, again in order of decreasing energies for the rotamer currently placed in the structure. Again, the rotamer with the best overall energy was retained for the final structure. More iterations rounds on the final result improved the overall rmsd (unpublished results), but we did not pursue this path<sup>39</sup> for the purposes of this paper.

We illustrate the effects of the doublet and singlet optimization stages by giving a specific example—Iaac, using the 1.0 Å rotamer library and optimal parameters (to be described in a later section). After the clash elimination stage, the rmsd between the predicted structure and the crystal structure was 0.733 Å. The pair clashes remaining in this case included the pairs F57 and L67, V37 and F82, and V43 and W45. Doublets optimization brought the rmsd down to 0.703 Å. The final singlet optimization stage brought the rmsd value further down to 0.622 Å.

For this case, doublet optimization took 3 s, while singlet optimization took 13 s. For comparison, clash elimination took 30 s to complete, while the rotamer self-energy calculation took 8 s.

**2.6. The Flat-Bottom Scoring Function.** Since our library is discrete, the best position for a side chain may lead to some contacts slightly too short. Since the VDW interactions become very repulsive very quickly for distances shorter than  $R_e$ , a distance too short by even 0.1 Å may cause a very repulsive VDW energy. This might lead to selecting an incorrect rotamer. In order to avoid this problem, we use a flat-bottom potential in which the attractive region is exactly the same down to  $R_e$ , but the repulsive region is displaced by some amount  $\Delta$  so that contacts that are slightly too short by  $\Delta$  will not cause a false repulsive energy. The form of this potential is shown in Figure 1.

We allow a different  $\Delta$  for each atom of each residue of each diversity. The way this is done is by writing  $\Delta$  as

$$\Delta = s \cdot \sigma$$

where  $s$  is a scaling factor, and the  $\sigma$  values are compiled as follows.

**2.6.1. Compilation of  $\sigma$  Values.** For each rotamer library we considered the 10 query protein structures in the HBPLUS set (see Materials and Methods). For each side

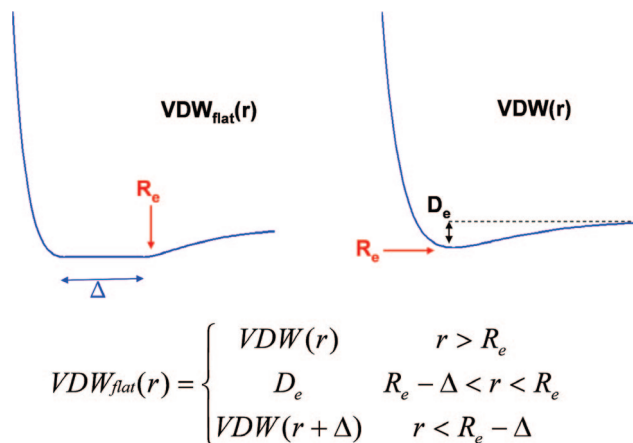


**Figure 1.** The flat-bottom potential. The inner wall is shifted by an amount  $\Delta$ .

**Table 2.**  $\delta$  and  $\sigma$  Values for Each Atom on the Arginine Side Chain, Listed in Order of Distance Away from the Main Chain<sup>a</sup>

dist. deviation (Å)	mean ( $\delta$ )	corrected error ( $\sigma$ )
C <sub>β</sub>	0.090	0.059
C <sub>γ</sub>	0.245	0.153
C <sub>δ</sub>	0.439	0.275
N <sub>ε</sub>	0.502	0.315
C <sub>ζ</sub>	0.588	0.369
N <sub>η1</sub> , N <sub>η2</sub>	0.858, 0.839	0.538, 0.526

<sup>a</sup> N<sub>η1</sub> and N<sub>η2</sub> are equivalent atoms; the average value is used in actual calculations. These numbers were obtained from the rotamer library of diversity 1.0 Å.

**Table 3.**  $\delta$  and  $\sigma$  Values for Each Atom on the Lysine Side Chain, Listed in Order of Distance Away from the Main Chain<sup>a</sup>

dist. deviation (Å)	mean ( $\delta$ )	corrected error ( $\sigma$ )
C <sub>β</sub>	0.089	0.056
C <sub>γ</sub>	0.259	0.162
C <sub>δ</sub>	0.406	0.254
C <sub>ε</sub>	0.596	0.373
N <sub>ζ</sub>	0.803	0.503

<sup>a</sup> These numbers were obtained from the rotamer library of diversity 1.0 Å.

chain in each query structure, we picked the closest matching rotamer (in rmsd) from the library and record the distance deviation for each atom of the side chain of that residue. Thus, the atoms at the tip of the longer side chains such as arginine and lysine would have greater distance deviations than C<sub>β</sub> atoms. The mean distance deviation ( $\delta$ ) for every atom of each amino-acid type over all 10 query proteins is then calculated. As an example, the  $\delta$  values for arginine and lysine rotamers in the rotamer library of 1.0 Å diversity (rotamer libraries were described in section 2.1) are listed in Tables 2 and 3.

We assume that the error in positioning of any one atom of the side chain will have a Gaussian distribution of the form

$$f(r) \propto e^{-\frac{r^2}{2\sigma^2}}$$

where  $r$  is the radial distance, and  $\sigma$  represents the standard deviation. Thus,

$$\rho(r) \propto 4\pi r^2 f(r)$$

is the probability of finding an atom at position  $r$  from the crystal position (which is weighted by a factor of  $4\pi r^2$  from the  $x$ ,  $y$ , and  $z$  distributions). The uncertainty  $\delta$  in the Cartesian distance along the line between two atoms is related to  $\sigma$  by the form

$$\delta = 2 \cdot \sqrt{\frac{2 \cdot \sigma^2}{\pi}}$$

where  $\delta$  is the value described above. This  $\sigma$  is listed for arginine and lysine in Tables 2 and 3.

**2.6.2. Scaling Factor  $s$ .** The  $\Delta$  values for each side-chain atom type will depend on their  $\sigma$  values:

$$\Delta = s \cdot \sigma$$

The deviations for  $\sigma$  above provide a measure of relative uncertainties in the ability of a library to describe the correct position of the side-chain atoms. However, to obtain the absolute value of the flat-bottomness we allow an overall scaling factor for the flat-bottom portion of the potential for all atoms.

The value of  $s$  was optimized for the Xiang set of 33 proteins for libraries of diversities ranging from 0.2 Å to 5.0 Å as discussed in section 3.

**2.6.3. Flat-Bottom Potential on Hydrogen Bond Terms.** We use a flat bottom for the VDW interactions and not for the Coulomb interactions because the VDW inner wall potential becomes repulsive very quickly with distance (e.g.,  $1/r^{12}$ ). Such scaling is not important for Coulomb since it scales as  $1/r$ . Most forcefields use a modified VDW interaction between hydrogen bonded atoms. Current version of AMBER and CHARMM do this between donor hydrogen and the acceptor heavy atom, treating the interaction as a standard 12–6 Lennard-Jones with modified parameters. The flat bottom for the other van der Waal interactions should apply equally well for these hydrogen bond terms. However, DREIDING uses an explicit 12–10 hydrogen bond term between the heavy atoms combined with a factor depending upon the linearity of the donor-hydrogen-acceptor triad

$$E_{hb} = D_{hb} [5(R_{hb}/R_{DA})^{12} - 6(R_{hb}/R_{DA})^{10}] \cos^4(\theta_{DHA})$$

where  $D_{hb}$  stands for the well-depth of the hydrogen bond potential,  $R_{hb}$  is the equilibrium distance, and  $\theta_{DHA}$  is the angle between the hydrogen bond donor atom, hydrogen, and the acceptor atom. We use a flat-bottom potential for this DREIDING hydrogen bond term. However, we now allow both the inner and outer walls to shift by an amount  $\Delta$  from the equilibrium point. The objective here is to also let the potential capture the polar contacts that would otherwise be missed, both when a donor–acceptor pair is too close or too far away from each other.

**2.6.4. Charges.** We use the CHARMM<sup>34</sup> charges for the protein and water, since these are standard and well-tested values. For ligands and other solvents, we use QEq<sup>40</sup> charges, which provide values similar to those from quantum mechanics.



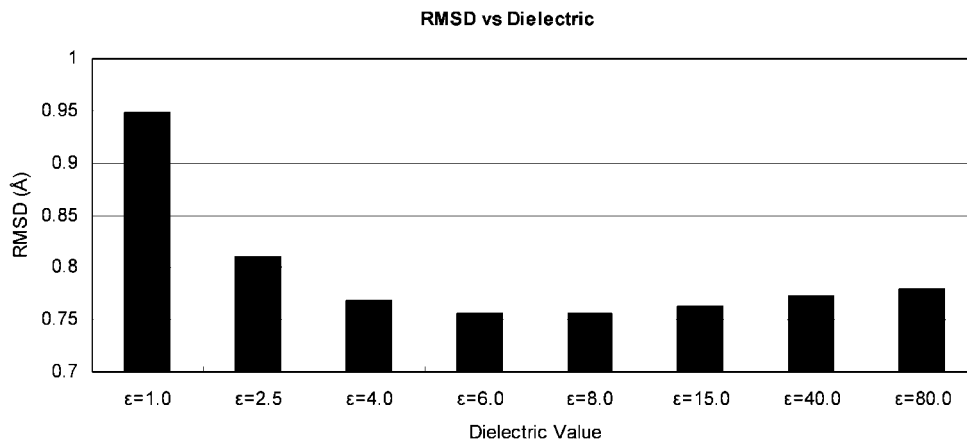


**Figure 2.** Effects on dielectric value on rmsd. The optimum value for the constant dielectric,  $\epsilon=6.0$  shown here, was obtained by fitting results for the Xiang set with a diversity of 1.0 Å and a scaling factor  $s$  of 1.0.

The Coulomb interaction between atoms 1 and 2 is written as

$$E_{\text{Coulomb}} = \frac{c_0 q_1 q_2}{\epsilon r_{12}}$$

where  $q_1$  and  $q_2$  are charges in electron units,  $r_{12}$  is in Å,  $\epsilon$  is the dielectric constant, and  $c_0 = 332.0637$  and converts to energies in kcal/mol. After optimization on a Xiang set of proteins using the 1.0 Å diversity rotamer library and a scaling factor  $s = 1.0$ , we chose the dielectric  $\epsilon=6.0$  (see Figure 2). Our calculation of electrostatics used a cubic spline cutoff beginning at 8 Å and ending at 10 Å.

**2.6.5. Total Rotamer Energies.** The valence energies (bonds, angles, torsions, and inversion) plus the internal HB, Coulomb, and VDW energies of the rotamers were calculated beforehand and stored in the rotamer library.

The final form of the scoring function is thus

$$E_{\text{Total}} = \sum_i E_{\text{EL}} + \sum_{i < j} E_{\text{Pair}}$$

where  $E_{\text{EL}}$  is the sum over internal energies and the backbone interaction energies as described in section 2.1 and

$$E_{\text{Pair}} = E_{\text{VDW}} + E_{\text{HB}} + E_{\text{Coulomb}}$$

is the total nonbond energy between all pairs of atoms between a pair of residues.

For any particular atoms  $i$  and  $j$ , the total flat-bottom correction  $\Delta_{ij}$  for the VDW and HB terms is obtained from the individual  $\Delta$  values of  $\Delta_i$  and  $\Delta_j$  using the relation

$$\Delta_{ij} = \sqrt{\Delta_i^2 + \Delta_j^2}$$

This value corresponds to the standard deviation from the convolution of two normal distributions with standard deviations  $\Delta_i$  and  $\Delta_j$ .

### 3. Results and Discussion

**3.1. Single Placement of Side Chains.** To explore the effect on placement accuracy of using flat-bottom potentials, we increased the scaling factor  $s$  from 0.0 (no scaling) to 2.0 in 0.1 increments. To isolate the effects of the scaling, we placed side chains one at a time onto the protein, in the

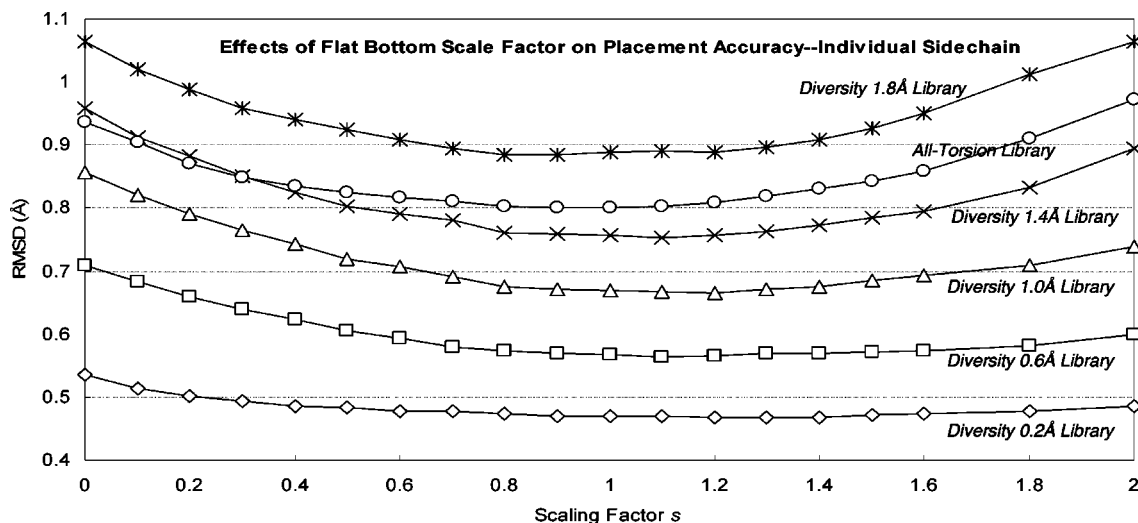
presence of all other side chains in their crystal positions. The values here represent the best possible results given a scoring function and a rotamer library.<sup>24</sup> The Xiang set of proteins described in Materials and Methods are used here.

Figure 3 shows that the best scaling factor is  $s \sim 1$  for all rotamer libraries. Note that  $s=1$  for the 1.0 Å library leads to an accuracy of 0.665 Å which is much better than the accuracy of 0.71 Å obtained using  $s=0$  (no scaling) for the much bigger 0.6 Å library.

Taking the all-torsion rotamer library as an example, the rmsd improves from 0.94 Å for  $s = 0$  (no flat bottom) to 0.80 Å for  $s = 0.9$ . This library with 378 rotamers leads to an accuracy of 0.80 Å, which compares with the accuracy of 0.75 Å obtained using the 1.4 Å library, which has 382 rotamers.

We optimized the scaling factors for rotamer libraries of diversities ranging from just 5.0 Å (44 rotamers) to 0.2 Å (13,000 rotamers). Tables 4 and 5 lists the optimum scaling factors and accuracies of these rotamer libraries, which lead to accuracies ranging from 0.47 Å (0.2 Å diversity) to 1.86 Å (5.0 Å diversity). We consider that the 1.0 Å library with an accuracy of 0.665 Å using 1014 total rotamers as a good compromise of efficiency and accuracy. These tables also list the results for the unscaled potential.

**3.2. Effects of Buried vs Exposed Residues.** The percentage of exposed residues considered in section 3.1 is only 25% because crystallographic waters and solvents were included in the calculation. We consider this as the best test of the scoring function. However, in practical applications, such water and solvent molecules will not be present. This creates additional uncertainties for the surface residues whose positions should be affected by the solvent and water. Without such solvent molecules, the energy functions will tend to distort the side chains to interact with other residues of the protein. Surface residues have more flexibility, and it would be better to have smaller scaling factors for these side chains. Thus, we optimized separate scaling factors for surface residues versus bulk. To do this, we calculated the SASA for the Xiang set and assigned all residues >20% exposed as surface. The resulting optimized scaling factors are in Table 6. In Figure 4, we see that the accuracy for the



**Figure 3.** Single side-chain placement accuracy for various rotamer libraries at different  $s$  values. Shown are the libraries of 0.2 Å diversity (14755 rotamers), 0.6 Å diversity (3195 rotamers), 1.0 Å diversity (1014 rotamers), 1.4 Å diversity (378 rotamers), 1.8 Å diversity (218), and all-torsion (382 rotamers). The coarser the rotamer library is, the more pronounced the effect of  $s$  becomes.

**Table 4.** Optimized  $s$  Value for Rotamer Libraries of Size Ranging from 0.2 Å to 5.0 Å, Plus the All Torsion Rotamer Library<sup>a</sup>

library	number of rotamers	unmodified potential (rmsd, Å)	best $s$ value	best rmsd (Å)
0.2 Å	14755	0.536	1.3	0.468
0.6 Å	3195	0.710	1.1	0.564
1.0 Å	1014	0.857	1.2	0.665
1.4 Å	378	0.958	1.1	0.753
1.8 Å	214	1.064	0.9	0.885
2.2 Å	136	1.343	0.8	1.175
3.0 Å	84	1.624	0.7	1.487
5.0 Å	44	1.890	0.7	1.860
all-torsion	382	0.937	0.9	0.800

<sup>a</sup> The  $s$  values for that gives the best RMSD value is listed.

**Table 5.** Effect of  $s$  Values on  $\chi_1/\chi_1 + 2$  Accuracy<sup>a</sup>

library	number of rotamers	$\chi_1/\chi_1 + 2$ accuracy from unmodified scoring function	best scaling factor $s$	$\chi_1/\chi_1 + 2$ accuracy using best $s$ value
0.2 Å	14755	95.0%/91.8%	1.3	96.3%/93.4%
0.6 Å	3195	92.6%/87.7%	1.1	95.6%/92.1%
1.0 Å	1014	90.0%/83.4%	1.2	95.3%/90.4%
1.4 Å	378	87.8%/80.0%	1.2	94.7%/88.9%
1.8 Å	214	84.3%/75.6%	1.2	91.5%/83.8%
2.2 Å	136	71.9%/61.0%	0.8	79.1%/68.0%
3.0 Å	84	63.4%/54.1%	0.7	68.4%/58.9%
5.0 Å	44	53.2%/44.9%	0.7	54.9%/45.8%
all-torsion	382	89.6%/81.3%	1.1	93.3%/86.8%

<sup>a</sup> Rotamer libraries of diversity ranging from 0.2 Å to 5.0 Å, plus the all-torsion rotamer library are used. The best  $\chi_1 + 2$  accuracy is used to determine the most effective scaling factor  $c$ . A  $\chi$  angle is considered correct if within 40° of the corresponding  $\chi$  angle in the crystal side-chain conformation.

1.4 Å library increases from 0.809 (bulk) and 1.409 (surface) to 0.515 Å (bulk) and 1.107 Å (surface).

The current SCREAM software does not distinguish between surface and bulk residues. In order to predict the surface residues prior to assigning the side chains, we

**Table 6.** Accuracy Comparison in Single Side-Chain Placements for Buried and Exposed Residues for the Xiang Test Set

rotamer library	optimal scaling factor $s$ for core residues	optimal scaling factor $s$ for surface residues	core residue rmsd (Å) for optimal $s$	surface residue rmsd (Å) for optimal $s$
0.2 Å	1.4	0.6	0.309	0.939
0.6 Å	1.2	0.8	0.414	1.010
1.0 Å	1.2	0.9	0.515	1.107
1.4 Å	1.3	0.8	0.605	1.171
1.8 Å	1.2	0.7	0.742	1.227
2.2 Å	0.8	0.6	1.105	1.371
3.0 Å	0.7	0.6	1.439	1.625
5.0 Å	0.7	0.7	1.835	1.935
all-torsion	0.9	0.8	0.656	1.224

recommend using the alanized protein and rolling a ball of 2.9 Å instead of the standard 1.4 Å (Supporting Information).

**3.3. Placement of All Side Chains on Proteins, Comparison with SCWRL.** The effectiveness of the flat-bottom potential in the single-placement setting extends to multiple side-chain placements. Based on the same Xiang test set of 33 proteins, we report the placement accuracy shown in Figure 5. The optimal  $s$  values were similar to the values from single placement tests. For example, the 1.0 Å library had an optimum scaling factor  $s=1.0$  leading to an accuracy of 0.747 Å (compared to 0.665 Å for single placement). Overall, the accuracy discrepancy in multiple placement and single placement setting comes to a 0.09 Å rmsd. Using the  $\chi_1/\chi_2$  criterion leads to similar conclusions, as seen in Table 8.

The overall improvement in rmsd of the optimal  $s$  values over the exact Lennard-Jones potential, however, is more dramatic than in the single placement tests. For instance, by introducing the optimal  $s$  value for the float-bottom potential, in the single side-chain placement case, the accuracy improved from 0.834 Å to 0.663 Å, an improvement of 0.17

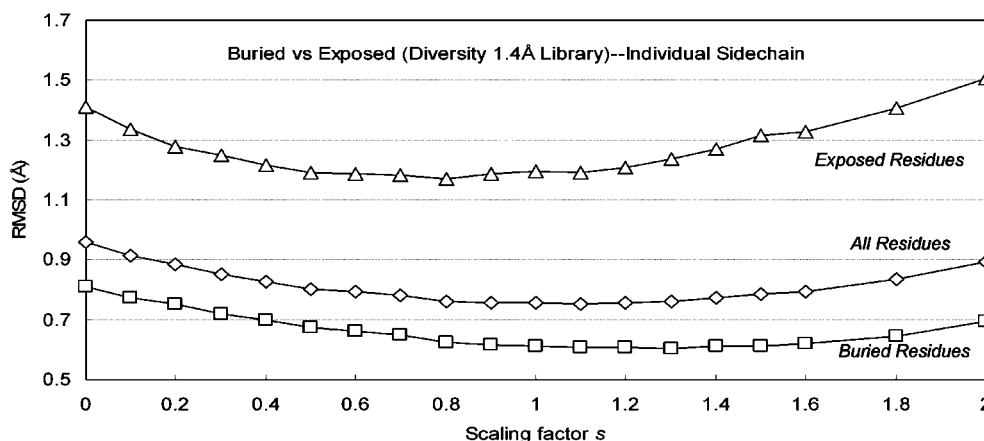


**Figure 4.** The effects of varying the scaling factor  $s$  on placement accuracies for the exposed and core residues. Shown are results from the 1.4 Å diversity rotamer library results. Exposed residues account for approximately 25% of all residues.

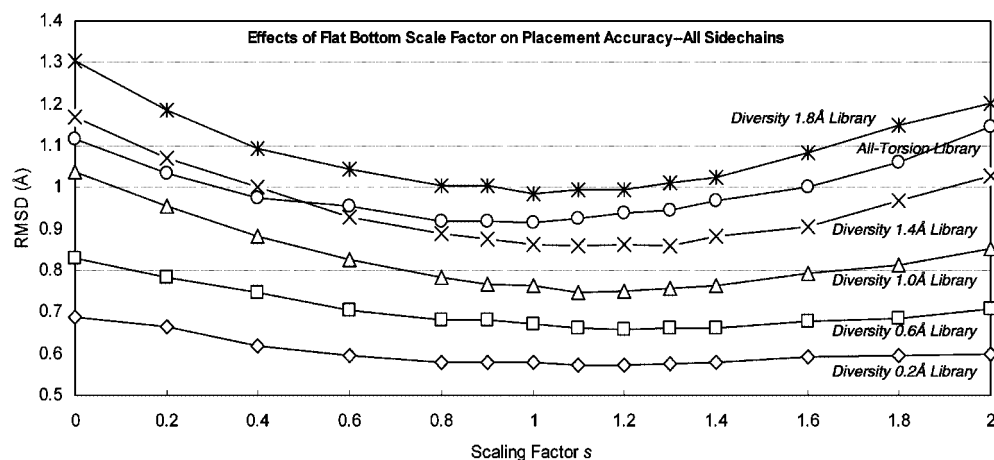


**Figure 5.** Accuracy for simultaneously replacing all side chains for various rotamer libraries at different  $s$  values. Shown are the libraries of 0.6 Å diversity (3195 rotamers), 1.0 Å diversity (1014 rotamers), 1.4 Å diversity (378 rotamers), 1.8 Å diversity (218), and all-torsion (382 rotamers).

**Table 7.** Optimized  $s$  Value for Rotamer Libraries of Size Ranging from 0.2 Å to 5.0 Å, Plus the All-Torsion Rotamer Library<sup>a</sup>

library	number of rotamers	unmodified potential (rmsd, Å)	best scale factor $s$ value	best rmsd (Å)
0.2 Å	14755	0.689	1.2	0.571
0.6 Å	3195	0.830	1.2	0.657
1.0 Å	1014	1.036	1.1	0.747
1.4 Å	378	1.171	1.1	0.860
1.8 Å	214	1.303	1.0	0.985
2.2 Å	136	1.545	0.9	1.278
3.0 Å	84	1.756	0.8	1.565
5.0 Å	44	1.987	0.6	1.909
all-torsion	382	1.118	1.0	0.916
SCWRL	0.951 Å			

<sup>a</sup> The scaling factor  $s$  that gives the best RMSD value is included. For comparison, SCWRL gives a RMSD of 0.95 Å for the same residues and proteins tested in this set.

Å; in the all-side-chain placement case, the improvements went from 1.024 Å to 0.755 Å, an improvement of 0.27 Å.

To compare our results with SCWRL, we applied SCWRL3.0 on the Xiang set of proteins. We found an accuracy of 0.85 Å for SCWRL. A direct comparison between SCREAM and SCWRL is difficult since SCWRL

**Table 8.** Effect of  $s$  Values on  $\chi_1/\chi_{1+2}$  Accuracy<sup>a</sup>

library	number of rotamers	$\chi_1/\chi_{1+2}$ accuracy from unmodified scoring function	optimal $s$ value	$\chi_1/\chi_{1+2}$ accuracy using optimal $s$
0.2 Å	14755	91.4%/86.6%	1.3	94.1%/89.9%
0.6 Å	3195	89.7%/83.0%	1.1	93.8%/88.5%
1.0 Å	1014	84.5%/75.6%	1.1	92.9%/86.7%
1.4 Å	378	81.7%/71.4%	1.3	92.1%/84.3%
1.8 Å	214	77.4%/67.3%	1.2	88.6%/80.0%
2.2 Å	136	66.8%/55.0%	1.1	75.7%/64.6%
3.0 Å	84	60.6%/50.5%	0.8	66.2%/56.7%
5.0 Å	44	52.1%/43.9%	0.6	54.3%/45.7%
all-torsion	382	85.0%/73.4%	1.0	89.7%/81.5%
SCWRL	86.4%/79.7%			

<sup>a</sup> Rotamer libraries of diversity ranging from 0.2 Å to 5.0 Å plus the all-torsion rotamer library are used. The best value for  $\chi_1/\chi_{1+2}$  correctness is used to determine the most effective  $s$  value. A  $\chi$  angle is considered correct if within 40° of the corresponding  $\chi$  angle in the crystal side-chain conformation. The  $\chi_1/\chi_{1+2}$  correctness for SCWRL is 86.4%/79.7%.

uses a backbone dependent rotamer library and a more sophisticated multiple side-chain placement algorithm. However, we note that the 1.8 Å SCREAM library, with just 214 rotamers, achieved an accuracy of 0.86 Å rmsd which is

**Table 9.** Average Energy Values for the 33 Proteins over Varying  $s$  Values<sup>a</sup>

$s$ value	0.6 Å library		1.0 Å library		1.4 Å library		all-torsion library	
	Starting energy	minimized energy	starting energy	minimized energy	starting energy	minimized energy	starting energy	minimized energy
0	-1234.3	-3163.1	546.8	-2839.2	6957.0	-2544.8	1558154.0	-2317.1
0.2	-2237.0	-3225.5	530.7	-2969.3	2804.0	-2675.2	1260675.0	-2515.2
0.4	-2195.1	-3271.3	417.6	-3053.8	<b>2610.3</b>	-2790.4	34774.5	-2767.6
0.6	<b>-2364.8</b>	-3312.2	<b>-624.4</b>	-3102.8	3454.9	-2871.2	<b>34628.7</b>	-2826.2
0.8	-2227.6	-3328.1	-419.9	-3168.6	4970.1	-2929.7	41225.3	-2849.5
0.9	-2130.1	-3325.0	-166.4	-3165.1	10013.7	-2941.8	166369.5	-2836.7
1.0	-2041.5	-3331.6	143.2	-3166.3	132017.6	<b>-2952.7</b>	173157.0	<b>-2854.6</b>
1.1	-1952.9	<b>-3341.3</b>	1431.4	<b>-3177.5</b>	136424.5	-2945.5	53846.7	-2845.7
1.2	-1764.6	-3338.9	1885.2	-3171.0	146372.5	-2938.1	62057.7	-2794.9
1.3	-545.0	-3327.5	3278.3	-3161.9	161903.0	-2919.4	101904.8	-2783.0

<sup>a</sup> All energy values include valence and nonvalence terms, and the units are presented in kcal/mol. The energies do not include interaction terms between atoms that are not involved in the side-chain placement calculations. Numbers in bold are the minimum values for each category.

**Table 10.** Average RMSD Values (in Å) for the Xiang Set of 33 Proteins, before and after Minimization<sup>a</sup>

scaling factor	0.6 Å library		1.0 Å library		1.4 Å library		all-torsion library	
	starting rmsd	minimized rmsd	starting rmsd	minimized rmsd	starting rmsd	minimized rmsd	starting rmsd	minimized rmsd
0	0.830	0.737	1.036	0.930	1.171	1.061	1.112	1.003
0.2	0.784	0.694	0.954	0.848	1.071	0.962	1.035	0.916
0.4	0.746	0.658	0.884	0.773	<b>1.003</b>	0.887	0.975	0.848
0.6	<b>0.706</b>	0.615	<b>0.827</b>	0.718	0.930	0.814	<b>0.954</b>	0.823
0.8	0.681	0.591	0.784	0.668	0.888	0.767	0.920	0.787
0.9	0.682	0.591	0.766	0.651	0.877	0.752	0.917	0.786
1.0	0.672	0.581	0.764	0.647	0.863	<b>0.736</b>	0.916	<b>0.780</b>
1.1	0.662	<b>0.569</b>	0.747	<b>0.625</b>	0.860	0.729	0.923	0.786
1.2	0.657	0.562	0.752	0.629	0.861	0.727	0.937	0.799
1.3	0.662	0.568	0.758	0.632	0.860	0.724	0.946	0.803

<sup>a</sup> Entries in bold correspond to those with the lowest DREIDING energies before and after minimization; see Table 9 for details.

comparable to the 0.85 Å for SCWRL, which has a rotamer for each major torsion angle, coming to  $\sim 370$  rotamers. Of course, SCWRL uses a backbone dependent rotamer library, so the specific torsion angles of those rotamers depend on the backbone  $\varphi$ - $\Psi$  angles.

**3.4. Effects of Minimization on Structures from Different Scaling Factors.** For efficiency in predicting the optimum combination of side-chain conformations, we use the discrete rotamers from the library with no minimization. Because of this, the closest rotamer in the library to the correct conformation may have short contacts. That is why we use the flat-bottom potential. Of course, after assigning the side chains we need to optimize the structures in preparation for docking and other applications. To assess how well this optimization improves the accuracy we have minimized the side chains for each structure for 100 steps (using DREIDING in vacuum) with the results in Table 9.

We see that the initial configurations often have very high energies, but after minimization these energies become fairly similar for different scaling factors with the same diversity. As expected, the best energies (in bold face) generally come from a scaling factor of 1.0 or 1.1. We note also that as the diversity of the library decreased, the energy of the final optimized configurations also decreased, indicating increased accuracy.

As expected, the rmsd also decreases as we minimize the structures. These results are shown in Table 10. For example, for the 1.0 Å library, accuracy improved from 0.747 Å to 0.625 Å.

**3.5. Program Execution Performance.** All tests have been run on Intel Xeon 2.33 GHz CPU single processors. The tradeoff in time vs rotamer library size is detailed in Table 11. Obviously, the size of rotamer libraries affects the time spent on side-chain placement. Compared to SCWRL, the time required by SCREAM is relatively slow. However, SCWRL does not explicitly include hydrogen atoms, and use of united atom should reduce the computational time by SCREAM by a factor of about three.<sup>36</sup>

It might appear that the increased accuracy of using SCREAM compared to SCWRL might not justify the increased expense. However, these test cases are all systems for which exact structures are available. We have found in applications involving predictions of new structures that the SCREAM procedure works better than SCWRL, in particular for predicting GPCRs, as will be presented elsewhere.<sup>41</sup>

**3.6. Tests on the Liang Set Using The Optimized Scaling Factor.** In the previous sections, we optimized the scaling factors for the Xiang set and discussed the accuracy for the Xiang set. As to better indicate how well SCREAM works for new systems we tested the predictions for the Liang set using the scaling factors optimized for the Xiang set.

Rotamer libraries of practical use, including those of diversities 0.6 Å, 1.0 Å, 1.4 Å, 1.8 Å, and the all-torsion rotamer library were used for this test. Results are shown in Table 12. For example, using the 1.4 Å library, we found an accuracy of 0.96 Å for all residues and 0.74 Å for the buried residues, which compares to 0.86 Å for all residues and 0.73 Å for the buried residues for the Xiang set. The



**Table 11.** Performance Measure of SCREAM, with Rotamer Libraries of Various Diversities<sup>a</sup>

library diversity	number of rotamers	time per protein	X <sub>1</sub> (%)		X <sub>1+2</sub> (%)		rmsd (Å)	
			buried	all	buried	all	buried	all
0.2 Å	14755	554 s	96.7	93.8	93.7	89.7	0.43	0.58
0.6 Å	3195	291 s	96.1	93.5	91.6	88.0	0.53	0.67
1.0 Å	1014	146 s	95.5	92.4	89.8	85.9	0.62	0.76
1.4 Å	378	110 s	94.4	91.6	87.0	83.8	0.73	0.86
1.8 Å	214	91 s	90.9	87.8	83.4	80.0	0.85	0.99
all-torsion	382	147 s	92.4	89.7	85.2	81.5	0.78	0.92
SCWRL	n/a	3 s	90.3	86.4	84.4	79.7	0.79	0.95

<sup>a</sup> The timing statistics were taken from the runs that gave the best energy values.

**Table 12.** SCREAM Predictions on the Liang Test Set Using Optimized Scaling Factor for Rotamer Libraries of Various Diversities<sup>a</sup>

library diversity	number of rotamers	run time per protein	χ <sub>1</sub> (%)		χ <sub>1+2</sub> (%)		rmsd (Å)	
			buried	all	buried	all	buried	all
0.6 Å/s = 1.2	3195	78.9 s	96.4	90.8	92.6	84.3	0.52	0.80
1.0 Å/s = 1.1	1014	41.0 s	93.6	89.1	87.1	80.7	0.69	0.93
1.4 Å/s = 1.1	378	29.9 s	94.5	89.4	86.2	79.9	0.74	0.96
1.8 Å/s = 1.0	214	27.6 s	90.3	85.2	83.5	77.0	0.84	1.05
all-torsion /s = 1.0	382	32.5 s	93.4	87.6	87.3	79.4	0.77	0.99
SCWRL	n/a	2 s	90.5	83.7	84.3	75.5	0.82	1.10

<sup>a</sup> The percentage of buried residues in this test set is about 40%, greater than the 25% figure from the previous test set. We include crystal structure solvents in the predictions, and the increase in exposed residues is due to the fewer resolved solvents in those structures.

**Table 13.** Effect of Different Lennard-Jones Potentials and Their Optimal Scaling Factor *s*<sup>a</sup>

LJ type	unmodified potential (rmsd, Å)	best scale factor <i>s</i> value	best scale factor rmsd (Å)
7–6	0.831	0.4	0.767
8–6	0.845	0.6	0.752
9–6	0.855	0.7	0.752
10–6	0.911	0.8	0.749
11–6	0.963	1.0	0.741
12–6	1.036	1.1	0.747

<sup>a</sup> Tests were done on the Xiang protein set using the 1.0 Å rotamer library.

reason for the decreased accuracy is that 40% of side chains in the Liang set are solvent exposed compared to 25% for the Xiang set. The prediction of core residues is approximately at the same level of accuracy as reported in previous sections.

**3.7. Parameters for Other Lennard Jones Potentials.** While the Lennard-Jones 12–6 potential is the most commonly used, it has been demonstrated that softer potentials improve placement accuracy.<sup>42</sup> Thus, we tested out Lennard-Jones potentials of the 7–6, 8–6, 9–6, 10–6, and 11–6 types on the 1.0 Å rotamer library for the Xiang protein set. As expected, the softer potentials performed better, but the results can be improved further by including a flat-bottom region in the potential. Results are shown in Table 13. The optimal value of the scaling factor *s* decreases with softer Lennard-Jones potentials, which was expected and was consistent with the flat-bottom potential approach. It is interesting to note that the 11–6 potential with optimized scaling factor *s* achieved the best overall rmsd value for this test, though the differences across the different Lennard-Jones potentials were small.

**3.8. Comparison with VDW Radii Scaling.** We also test out using reduced VDW radii values on the 1.0 Å rotamer library for the Xiang protein set. The results are shown in

**Table 14.** Effects of VDW Scaling<sup>a</sup>

VDW radii scaling	rmsd (Å)
75%	0.959
80%	0.884
85%	0.866
90%	0.896
95%	0.956
100%	1.036

<sup>a</sup> Tests were done on the Xiang protein set using the 1.0 Å rotamer library.

Table 14. The improvement from using reduced VDW radii is not as pronounced as the improvement from using softer Lennard-Jones potential forms, described in the previous section.

**3.9. Extension beyond the Natural Amino Acids.** The  $\sigma$  values were calculated for the natural amino acids. To extend the flat-bottom potential approach for ligands and non-natural amino acids, a value for  $\Delta$  or  $\sigma$  needs to be determined. These values clearly depend on how conformations were generated, but we recommend a simple scheme such as using  $\Delta = 0.4$  Å for all atoms.

## 4. Conclusion

We show that side-chain placement using a flat-bottom potential leads to excellent side-chain placement results with a simple combinatorial side-chain placement algorithm. We present a straightforward method for deriving these parameters and applied this to rotamer libraries with a wide range of diversities (0.2 Å to 5.0 Å). The potential is a simple modification of a Lennard-Jones potential, making it easy to incorporate into existing software.

A particularly important application for side-chain placement is in protein folding applications where one wants to find rapidly the best side-chain positions for each backbone configuration. A first application of SCREAM for such

problems is the recent development of the MembSCREAM methodology for predicting three-dimensional structures for G-Protein Coupled Receptors.<sup>41</sup>

**Acknowledgment.** We want to thank Professor Nagrajan Vaidehi (City of Hope) and Dr. Ravinder Abrol for many insightful suggestions. We would also like to thank Mr. Caglar Tanrikulu, Mr. Peter Kekenyes-Huskey, and Mr. Adam R. Griffith for testing, using, and pointing out improvements while using the software. This research was supported partially by NIH (R21-MH073910-01-A1) with additional support from DARPA-PROM. The computational facilities were provided by DURIP grants from ARO and ONR.

**Supporting Information Available:** Contact information for the current SCREAM software and prediction of surface residues prior to side-chain assignment. This material is available free of charge via the Internet at <http://pubs.acs.org>.

## References

- Trabanino, R. J.; Hall, S. E.; Vaidehi, N.; Floriano, W. B.; Kam, V. W. T.; Goddard, W. A. *Biophys. J.* **2004**, *86* (4), 1904–1921.
- Vaidehi, N.; Kalani, Y. S.; Hall, S. E.; Freddolino, P. L.; Trabanino, R. J.; Floriano, W. B.; Spijker, P.; Goddard, W. A. *Biophys. J.* **2005**, *88* (1), 357A–357A.
- Vaidehi, N.; Floriano, W. B.; Trabanino, R.; Hall, S. E.; Freddolino, P.; Choi, E. J.; Zamanakos, G.; Goddard, W. A. *Proc. Natl. Acad. Sci. U.S.A.* **2002**, *99* (20), 12622–12627.
- Malakauskas, S. M.; Mayo, S. L. *Nat. Struct. Biol.* **1998**, *5* (6), 470–475.
- Kraemer-Pecore, C. M.; Lecomte, J. T. J.; Desjarlais, J. R. *Protein Sci.* **2003**, *12* (10), 2194–2205.
- Dwyer, M. A.; Looger, L. L.; Hellinga, H. W. *Science* **2004**, *304* (5679), 1967–1971.
- Brooijmans, N.; Kuntz, I. D. *Annu. Rev. Biophys. Biomol. Struct.* **2003**, *32*, 335–373.
- Jacobson, M. P.; Pincus, D. L.; Rapp, C. S.; Day, T. J. F.; Honig, B.; Shaw, D. E.; Friesner, R. A. *Proteins: Struct., Funct., Bioinf.* **2004**, *55* (2), 351–367.
- Al-Lazikani, B.; Jung, J.; Xiang, Z. X.; Honig, B. *Curr. Opin. Chem. Biol.* **2001**, *5* (1), 51–56.
- Pierce, N. A.; Winfree, E. *Protein Eng.* **2002**, *15* (10), 779–782.
- Ponder, J. W.; Richards, F. M. *J. Mol. Biol.* **1987**, *193* (4), 775–791.
- Koehl, P.; Delarue, M. *J. Mol. Biol.* **1994**, *239* (2), 249–275.
- Mendes, J.; Soares, C. M.; Carrondo, M. A. *Biopolymers* **1999**, *50* (2), 111–131.
- Vasquez, M. *Biopolymers* **1995**, *36* (1), 53–70.
- Kussell, E.; Shimada, J.; Shakhnovich, E. I. *J. Mol. Biol.* **2001**, *311* (1), 183–193.
- Desmet, J.; Demaeyer, M.; Hazes, B.; Lasters, I. *Nature* **1992**, *356* (6369), 539–542.
- Lasters, I.; Demaeyer, M.; Desmet, J. *Protein Eng.* **1995**, *8* (8), 815–822.
- Pierce, N. A.; Spriet, J. A.; Desmet, J.; Mayo, S. L. *J. Comput. Chem.* **2000**, *21* (11), 999–1009.
- Looger, L. L.; Hellinga, H. W. *J. Mol. Biol.* **2001**, *307* (1), 429–445.
- Eisenmenger, F.; Argos, P.; Abagyan, R. *J. Mol. Biol.* **1993**, *231* (3), 849–860.
- Xiang, Z. X.; Honig, B. *J. Mol. Biol.* **2001**, *311* (2), 421–430.
- Liang, S. D.; Grishin, N. V. *Protein Sci.* **2002**, *11* (2), 322–331.
- Peterson, R. W.; Dutton, P. L.; Wand, A. J. *Protein Sci.* **2004**, *13* (3), 735–751.
- Petrella, R. J.; Lazaridis, T.; Karplus, M. *Fold. Des.* **1998**, *3* (5), 353–377.
- Mayo, S. L.; Olafson, B. D.; Goddard, W. A. *J. Phys. Chem.* **1990**, *94* (26), 8897–8909.
- DeMaeyer, M.; Desmet, J.; Lasters, I. *Fold. Des.* **1997**, *2* (1), 53–66.
- Lovell, S. C.; Word, J. M.; Richardson, J. S.; Richardson, D. C. *Proteins: Struct., Funct., Genet.* **2000**, *40* (3), 389–408.
- Dahiyat, B. I.; Mayo, S. L. *Proc. Natl. Acad. Sci. U.S.A.* **1997**, *94* (19), 10172–10177.
- Kuhlman, B.; Baker, D. *Proc. Natl. Acad. Sci. U.S.A.* **2000**, *97* (19), 10383–10388.
- Desjarlais, J. R.; Handel, T. M. *Protein Sci.* **1995**, *4* (10), 2006–2018.
- Wernisch, L.; Hery, S.; Wodak, S. J. *J. Mol. Biol.* **2000**, *301* (3), 713–736.
- Mendes, J.; Baptista, A. M.; Carrondo, M. A.; Soares, C. M. *Proteins: Struct., Funct., Genet.* **1999**, *37* (4), 530–543.
- Canutescu, A. A.; Shelenkov, A. A.; Dunbrack, R. L. *Protein Sci.* **2003**, *12* (9), 2001–2014.
- Brooks, B. R.; Brucoleri, R. E.; Olafson, B. D.; States, D. J.; Swaminathan, S.; Karplus, M. *J. Comput. Chem.* **1983**, *4* (2), 187–217.
- Dunbrack, R. L.; Karplus, M. *J. Mol. Biol.* **1993**, *230* (2), 543–574.
- Jain, T.; Cerutti, D. S.; McCammon, J. A. *Protein Sci.* **2006**, *15* (9), 2029–2039.
- Vriend, G. *J. Mol. Graph.* **1990**, *8* (1), 52–&.
- Schüttelkopf, A. W.; van Aalten, D. M. F. *Acta Crystallogr., Sect. D: Biol. Crystallogr.* **2004**, *60*, 1355–1363.
- Holm, L.; Sander, C. *Proteins: Struct., Funct., Genet.* **1992**, *14* (2), 213–223.
- Rappe, A. K.; Goddard, W. A. *J. Phys. Chem.* **1991**, *95* (8), 3358–3363.
- Abrol, R.; Kam, V. W. T.; Jenelle, B.; Wienko, H.; Goddard, W. A., unpublished.
- Grigoryan, G.; Ochoa, A.; Keating, A. E. *Proteins: Struct., Funct., Bioinf.* **2007**, *68* (4), 863–878.